# Two-dimensional granular Poiseuille flow on an incline: Multiple dynamical regimes

J.-C. Tsai,[1,2] W. Losert,[1,*] G. A. Voth,[1] and J. P. Gollub[1,2,†]
[1]*Department of Physics and Astronomy, Haverford College, Haverford, Pennsylvania 19041*
[2]*Department of Physics and Astronomy, University of Pennsylvania, Philadelphia, Pennsylvania 19104*
(Received 31 May 2001; published 19 December 2001)

We investigate experimentally the flow of a monolayer of spherical beads through a channel on a smooth incline that is bounded by rough sidewalls. Using high-speed video imaging and particle tracking, we measure the positions and velocities of all particles in the field of view. We find that the flows are accelerating and dilute if the channel exit is open. On the other hand, if the exit is constricted, flows can reach a state in which the local time-averaged velocity is invariant along the stream. In the latter case, we find a continuous transition from an oscillatory two-phase flow (2PF) regime with wide density variations to a uniform dense flow regime, depending on the channel width and the mean flow speed. These two regimes exhibit distinct density variation, time regularity, and transverse profiles. The rough sidewalls are found to be necessary for the 2PF regime. In the dense regions of both flows, particles exhibit temporary arches, long-range correlated velocities, inhomogenuous propagation of disturbances, and hexagonal lattice structures. On the other hand, the dilute regions of the two-phase flow are nearly collisionless. Existing models can neither fully describe the dynamics of both the dense and the dilute regions nor explain the spontaneous switching between them.

DOI: 10.1103/PhysRevE.65.011306 PACS number(s): 45.70.Vn, 83.50.Ha

## I. INTRODUCTION

The response of granular material to shear forces is important in characterizing granular dynamics. Poiseuille flows in a pipe or a channel have been a prominent model system for developing our understanding of shear flows in both ordinary fluids and granular materials. In addition, such flows frequently appear in material processing. A simplified case that is particularly convenient for laboratory investigation is that of two-dimensional channel flow driven by gravity. In this case, the source of energy is well defined, and the velocities of all the grains are easily measurable. The roughness of the channel boundary applies shear forces to the flow and the response can be studied in detail.

In this paper, we report an investigation of the flow of a monolayer of spherical beads rolling down a smooth incline. The flow is confined between two bumpy sidewalls, which form a channel geometry with a rough boundary condition. Using fast video imaging and particle tracking techniques, we obtain the positions and velocities of all particles in the field of view with excellent time resolution. These measurements enable us to analyze both the coarse-grained properties of the flow and its microscopic structure.

In previous studies of granular channel flows, experimentalists have generally observed that inhomogeneous oscillatory flows occur in narrow channels with high flow velocity, and that dense uniform solidlike flows occur when the channel is wide or the flow is slow. In the present system, by varying the dimensions of the channel and the exit, we are able to create flows with a wide range of mean density and velocity. We have carefully studied the continuous transition between two distinct and qualitatively different regimes, an oscillatory two-phase flow (2PF) regime in which the density varies widely, and a uniform dense flow (UDF) regime. Our investigations address several questions: How does the flow respond to the shear imposed by the sidewalls? Does a terminal velocity exist in an open channel? Can a uniform steady flow be obtained in an exit-constricted channel? What parameters control the flow profile, its time dependence, and the spatiotemporal pattern of density? What is the microscopic structure of the flow? Can we model its macroscopic behavior using the paradigm of standard binary collision theories? The results may be useful in constraining models of granular flows in the transitional regime where both collisions and friction are important. In the rest of this Introduction we review certain previous experiments and relevant theoretical contributions.

### A. Previous experiments

Studies of Poiseuille flows in vertical channels wider than tens of particle diameters have focused primarily on the nearly steady, time-averaged transverse profiles of uniform dense flows. The typical flow velocities were less than 10 cm/s. Nedderman and Loahakul [1] used a movie camera to determine the average velocity profile of a thin layer of millimeter-sized glass ballotini, kale, or mustard seeds. With roughened sidewalls, they found a profile consisting of a pluglike velocity plateau and two shear bands 6–8 beads wide. Savage [2,3] investigated the flow of millimeter-sized glass beads through a rectangular channel with two rough walls and two polished covering surfaces. He cross correlated the time signals from two slightly separated fiber optic sensors on one of the polished surfaces to determine the time-averaged velocity and transverse profile. Plug-flow profiles were also found, although Savage pointed out [2] that the flows might contain three-dimensional (3D) convection due to the interaction with the covering surfaces in some cases. A more recent work by Pouliquen and Gutfraind [4]

*Present address: Physics Dept., Univ. of Maryland, College Park, MD.
†Electronic mail: jgollub@haverford.edu

 

eliminated the effect of the confining surfaces by investigating the flow of long circular cylinders sandwiched between rough sidewalls. Their flows had mean velocity $\ll 0.1$ cm/s and belonged to a ''quasistatic'' regime defined in Sec. I B. Plug-flow profiles with shear bands were reported. Similar velocity profiles were obtained by Hunt and co-workers [5,6] using fiber optic techniques; video images of dyed particles were also utilized to study the anisotropy of velocity fluctuations and the self-diffusion of individual grains.

On the other hand, granular flows through narrow geometries were found to exhibit density waves. Dimon and coworkers [7–9] studied monolayer brass beads rolling through a long, small-angle narrow funnel on an incline. They treated the spatiotemporal pattern of density and velocity as 1D problems; the acceleration of individual particles and the creation and interaction of density-velocity waves were discussed; comparisons to traffic flows were made. Raafat *et al.* [10] studied density waves in the flow of 0.2-mm glass beads through vertical pipes with diameter ranging from 6 to 30 bead diameters; in their work, the creation of the waves was attributed to the interaction with the interstitial gas.

A recent study by Reydellet *et al.* [11] considered vertical chute flows with intermediate channel widths. Monolayer flows were confined between smooth transparent plates with rough lateral walls. Both steady flows and density waves were found, depending on the channel width.

### B. Theories and models

Savage [3] proposed that there are two limiting cases of granular flows: (a) a ''fully dynamic, fluidlike grain-inertia regime,'' corresponding to the situations named in Bagnold's classic work on solid-fluid mixtures [12], and (b) the ''quasistatic, rate-independent plastic regime.'' Case (a) is characterized by high shear rates, low concentration, and the dominance of binary collisions, in which only two grains can be simultaneously in contact. This is often modeled by kinetic theories resembling the classical treatments of molecular gases. Case (b) is the other limiting situation characterized by the vanishing shear rate, high concentration, and Coulomb-type friction. In this regime, most of the grains experience multiple contacts, meaning they are simultaneously in contact with more than one neighboring grain. Most practical granular flows are in a transitional regime, belonging to neither of the limiting cases; this fact was also discussed by Campbell [13]. In a recent study by Luding [14], an equation of state was proposed to describe 2D elastic granular gases that have a wide range of density, including the extremely dense regime where the crystalline order becomes important.

Steady-state profiles of granular Poiseuille flows have been modeled under various assumptions. Based on collisional dynamics corresponding to regime (a), Hui and Haff [15] derived the steady-state transverse profiles. However, the profiles obtained were sensitive to several free parameters related to material properties and boundary conditions, which resulted in difficulties in the comparison with experiments. The model of Pouliquen and Gutfraind [4] explained the flows in their experimental system, which belonged to the quasistatic regime (b). In a more recent paper [16], Savage proposed a model that incorporated both collision and Coulomb-type friction. By leaving the slip velocity and the density at the wall as two free parameters, he obtained solutions of the steady-state profile numerically. This paper also contains an in-depth review of previous theoretical models of granular flows.

Analyses of instability and density waves in infinitely long channels have been proposed. Valence and LePennec [17] analyzed the instability of a 1D problem defined by a cross-channel average of a continuum model. The continuum model assumed the collisional dynamics as in regime (a) and an energy-momentum balance at the bumpy sidewalls [18]. They predicted a channel-width-independent critical density, below which the corresponding base states would become unstable. Their nonlinear analysis concluded that the oscillation becomes more regular (''wavelike'') when the channel is narrow or the dissipation is strong, and becomes more irregular (''chaotic'') when the conditions are otherwise. Another paper by Wang *et al.* [19] gives a linear stability analysis of the 2D version of this problem. Their model adopted the same collisional dynamics except with flat frictional walls and predicted that the most unstable mode may switch to different branches, depending on the combination of the mean density and channel width.

In addition to the continuum models mentioned above, event-driven molecular dynamics (MD) simulations of collisional granular flows through 2D vertical channels have been performed. The simulation of narrow-channel flows [20] showed the occurrence of density waves, which are discussed in Sec. IV B. Wide-channel flows with the spin of individual disks taken into account were studied in Ref. [21]; comparisons with experiments in a 2D cell with an abruptly removed bottom were provided in Ref. [22].

In considering suitable models for our inclined flows, it is important to keep in mind the possible complications due to the rolling of the particles. It has been pointed out [23,24] that spheres rolling on a substrate may undergo extraordinary dissipation due to the sliding friction and may not be modeled simply by including a lower coefficient of restitution. This fact may cause our system to behave somewhat differently from monolayer vertical channel flows.

## II. EXPERIMENTAL SETUP

The flowing grains are hard-carbon steel spheres with diameter $d=0.3175$ cm, grade 1000 ($1000\times10^{-6}$ in. deviation from sphericity). They roll on a substrate of flat, conductive PVC plate, which prevents electrostatic charging of particles. The experimental system is schematically shown in Fig. 1. The inclination angle is adjustable; however, the practical working range is from 1° to 6°. Below 1°, clustered beads tend to establish a static equilibrium on the incline. The static force can come from surface cohesion, from the static friction between multiply contacting beads and the inclined surface, or both. Above 6°, colliding particles tend to create significant out-of-plane motion or even form multiple layers. Our investigations have focused on flows with inclinations between 2° and 4°, where beads are either experiencing slid-

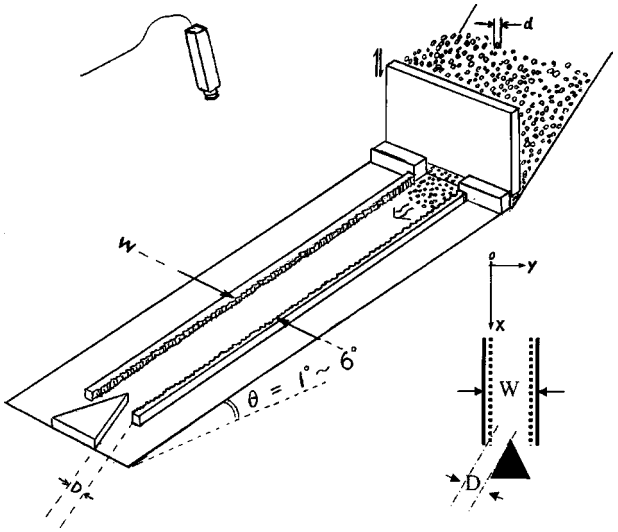


FIG. 1. The inclined channel and the definition of the geometrical parameters *W* and *D*.

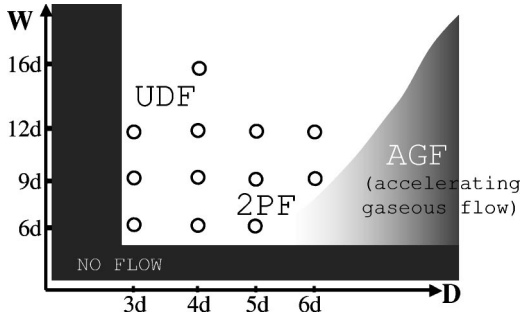


FIG. 2. Phase diagram. *W* is the width of the channel, and *D* is the size of the exit. The circles denote points where measurements were made. The gray scale represents the fact that the transition from 2PF to AGF has a certain degree of hysteresis so that the boundary drawn is merely schematic. The change from UDF to 2PF is continuous from upper left to bottom right.

ing friction against each other as they roll down collectively, or are colliding with each other without enduring contacts.

A hopper supplies the flowing grains. Its bottom plate and the connection with the inlet of the channel are designed to be adjustable in order to fine tune the initial velocity of the inflow, although in the present study we have kept the inflow condition fixed.

The rough boundaries are made of straight gear racks with regularly spaced notches of $\approx 0.50$ cm. One bead is glued to each notch so that about half of the bead protrudes. By doing so, we obtain two boundaries with a roughness comparable to the bead diameter.

The channel width *W* is adjustable, ranging from zero to more than $20d$. Since the roughness is about 0.5 particle diameter on each side, we define *W* as the maximum transverse separation that the centers of flowing beads can have in the channel. A movable triangular obstacle is positioned at the end of the channel. The outflow or exit dimension *D* is defined as the distance from the end of either rack to the nearest edge of the obstacle. The whole channel is about 120 cm long. When there is sufficient inflow, *W* and *D* determine the behavior of the system. We thus define $(W,D)$ as the parameter space. The entire channel is filled with a monolayer of beads before the exit is opened to initiate flow.

We use a Kodak Motion Corder fast video camera to capture time sequences of the flow. At a frame rate of 125 frame/s, we are able to capture up to 1092 images (8 bit $\times 512$ pixels$\times 240$ pixels) in real time. The images are analyzed to determine the trajectories and velocities of all particles in the sequential images, using codes written in IDL [25]. To determine particle trajectories, we find the Gaussian centroid to identify the centers of the bright spots, and then relate the spots in consecutive frames by choosing the one out of all possible connections that minimizes the total displacement [26]. At a typical magnification for which the bead diameter $d=16.8$ pixels, the position error is estimated to be less than $0.012d=38$ $\mu$m and the corresponding velocity error is less than 0.5 cm/s.

## III. EXPERIMENTAL RESULTS

The properties under investigation cover both coarse-grained quantities and individual motions, and may have both temporal and spatial dependence. We define certain terms and use them consistently throughout this paper. If not specified otherwise, a ''mean'' or ''local'' quantity always stands for an instantaneous coarse-grained average over a region containing tens of beads. We shall use the word ''variation'' in referring to the time dependence of a local coarse-grained quantity. An ''oscillation'' or ''wave'' means the variation with time around a certain average value but does not imply periodicity. The term ''fluctuation'' will be reserved for representing deviation of individual bead velocities from their local mean. The ''longitudinal'' direction $(x)$ means the one along the flow and ''transverse'' $(y)$ means the direction across the channel.

The density of beads refers to the 2D number density and is by itself a coarse-grained quantity. $\rho_{cp}$ stands for the density corresponding to a close-packed hexagonal lattice of uniformly sized round beads.

### A. Phase diagram and transition

A certain range of $(W,D)$ produces ''fully developed flows''—in the sense that the time-averaged local velocity does not increase down the channel. In Fig. 2, we show a typical phase diagram at an inclination angle of 2 °. Before continuing, we recommend that readers visit our web site [27] to see MPEG movies of the typical uniform dense flow (UDF), two-phase flow (2PF), accelerating gaseous flow (AGF), and flow around an obstacle. The behavior shown in the movies does not qualitatively change with inclination angle. The flow completely stops when either the channel width *W* or the exit opening width *D* is too small. This results from permanent jams that form in the channel or at the exit. On the other hand, when the obstacle is absent or when *D* is sufficiently large, the particles accelerate down the channel. In this case, the flow is dilute so that the typical mean free path—in the sense of a local Lagrangian frame

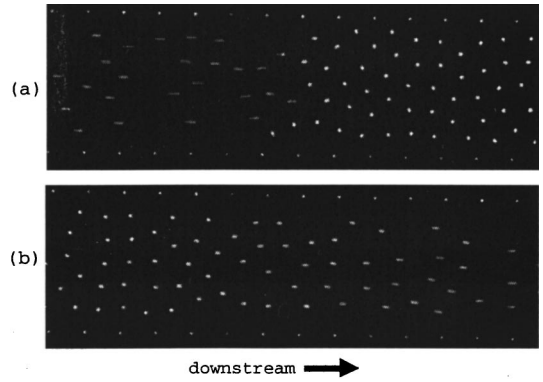


FIG. 3. Images of an oscillatory 2PF: the regularly spaced spots at the edges of both images are the glued beads on the sidewalls; a longer time of exposure was deliberately used in order to show the velocities of particles. (a) An interface of density discontinuity occurred at the upstream side of the dense regions. (b) The density changes continuously at the downstream side of the dense region, with the particles being gradually released.

where the average velocity of all nearby particles under consideration is zero—is larger than tens of bead diameters. We refer to this state as an AGF. Even if one attempts to initiate the flow from a completely jammed condition, the flow transforms itself into AGF: the process usually starts with the occurrence of dilute regions near the exit, which quickly extend over the entire channel.

The range of $(W,D)$ for the fully developed flows is denoted by the white area in the phase diagram. There are qualitative differences compared to the AGF in that (1) the average density is typically higher and (2) the time-averaged properties are constant along the channel. Moreover, we also observe gradual changes of features within this fully developed region, among which the most striking is the continuous increase in the amplitude of density waves: from UDF at the upper left of the white area to oscillatory 2PF at the lower right. At the 2PF limit, density waves repeatedly occur and propagate upwards. This can be visualized in Fig. 3: an abrupt change of density due to local congestion is clearly identifiable [Fig. 3(a)]; however, the relaxation of material from a dense region on its downstream side does not have a clear-cut interface [Fig. 3(b)]. On the other hand, at the UDF limit, particles tend to form close-packing crystals and to creep as solids do. The visualization of UDF is included in Sec. III D.

Quantitatively, the amplitude of density waves is determined by calculating the long-time rms density variation normalized by $\rho_{cp}$. The coarse-graining box has a width approximately equal to the channel width and a length $\approx 9d$ in the flow direction. The particle counting is linearly smoothed across the four edges of the box in order to eliminate noise due to discreteness. We have found that the wave amplitude increases with larger opening $D$, but decreases with wider channel width $W$. Both dependencies are monotonic with the other parameter held fixed, as shown in Fig. 4.

When a fully developed flow is sustained with the channel width fixed, the opening $D$ serves as a control valve that determines the mean flow rate and the time-averaged cross-

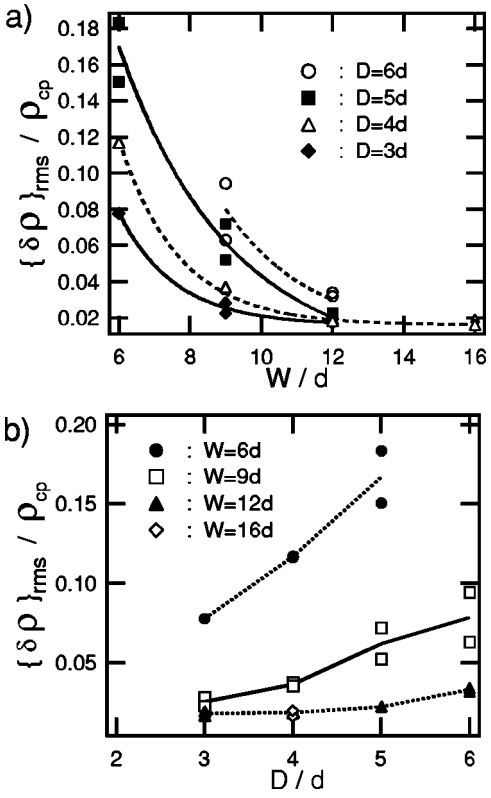


FIG. 4. Long-time rms density variation as a function of geometrical confinement factors. The data points correspond to the circles in Fig. 2 and the lines are drawn to guide the eye. The density is normalized in units of the 2D close-packing density $\rho_{cp}$. The change of rms density variation is found to be monotonic with either $W$ or $D$.

channel mean velocity everywhere upstream. By including the velocity information, we present in Fig. 5 the rms density variation as function of time-averaged mean velocity, for several different channel widths. We find that (1) at constant channel width, the density wave amplitude increases with increasing mean flow velocity and (2) the density variation

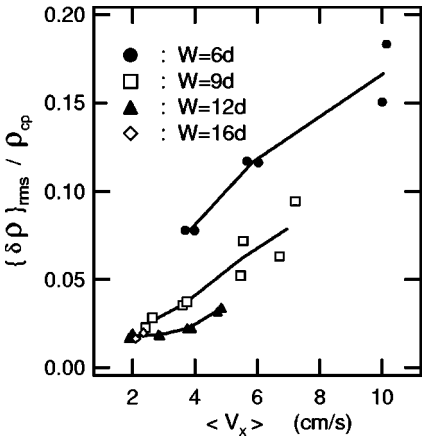


FIG. 5. Long-time rms density variation as a function of time-averaged mean velocity $\langle V_x \rangle$, at different channel widths $W$. The data points correspond to the circles in Fig. 2 and the density is normalized in units of the 2D close-packing density $\rho_{cp}$.

increases dramatically as the channel becomes narrower.

We also did tests with the rough sidewalls replaced by flat steel bars, keeping the channel widths and the mean velocities approximately the same in order to make comparisons. Over the entire range of our investigation, the flows are always uniform and dense with irregular velocity oscillations; the behavior is similar to that of the UDF regime in the phase diagram of Fig. 2.

Our measurements suggest that the rough boundary is a necessary condition for producing significant density waves, with the 2PF being its extreme case. We present additional information on the interaction of particles with the boundaries in Sec. III C.

### B. Oscillatory Behavior

We calculate the local mean velocity, density, and the rms fluctuations of the two velocity components as a function of time. Three observation boxes located adjacent to each other along the channel were chosen in order to measure the time variation of these local quantities; the size and edge smoothing of each box is the same as used in Sec. III A.

The time dependence of a typical 2PF is shown in Fig. 6. The velocity and density oscillate coherently, corresponding to the development of jamming and un-jamming in each observation box. The oscillation of the 2PF appears to have a characteristic frequency, although it is not perfectly regular. The abrupt change of mean velocity and density corresponds to the passing of the upward moving interface of density discontinuity [shown in Fig. 3(a)] through each observation box. On the other hand, the asymmetry of the time variation is the consequence of the fact that the relaxation of beads takes place continuously, as is shown in Fig. 3(b). The time lags between the three different observation boxes in Fig. 6(a) show that the velocity and density variations propagate upward at about 14 cm/s in this case ($W=6d, D=5d$).

Note that the local velocity fluctuations [Fig. 6(c)], which correspond to the square root of the ''granular temperature'' defined in the context of kinetic theories, are large only when the interfaces pass the observation region. In addition, the typical density in the dilute regions is so low that the corresponding mean free path appears to be longer than the channel width; our visual examination of video data (shown in web movies and Fig. 3) also suggests that, in an averaged sense, particles in the dilute regions experience less than one collision before reaching the next front line of dense region. Similar density, velocity, and granular temperature fields are found in monolayer flows in long, small-angle funnels and are reported in recent work by Hørlück and Dimon [9].

The contrasting time dependence of a typical UDF is shown in Fig. 7(a). There exists considerable oscillation of the mean velocity in the UDF, as in the 2PF. However, the UDF has a time variation far more irregular than the 2PF. The typical amplitude of oscillation of mean velocity is larger than the local velocity fluctuations; the oscillations of mean velocity in the three boxes are almost simultaneous. These facts indicate that the beads' motions are instantaneously correlated with a length scale at least a few times the longitudinal size of the adjacent observation boxes, which

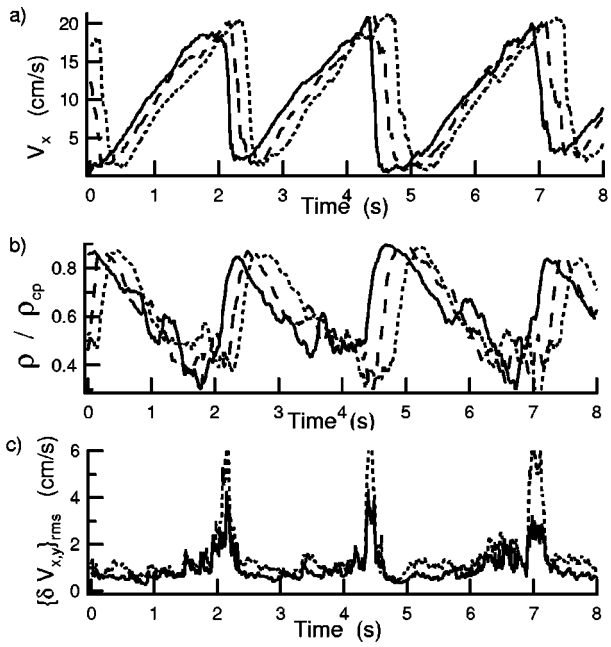


a,b) Mean velocity ($V_x$) and density ($\rho$) in three boxes along the channel:
------upstream, – – middle, ——downstream
c) RMS velocity fluctuations (the downstream box only) :
------longitudinal ( $\{\delta V_x\}_{rms}$ ) , ——transverse ( $\{\delta V_y\}_{rms}$ )

FIG. 6. Time dependence of an oscillatory 2PF with $W=6d$ and $D=5d$. The density is normalized in units of the 2D close-packing density $\rho_{cp}$. (a) The density and local mean velocity vary coherently; the time lags between signals of different observation boxes along the longitudinal direction indicate an upward propagation speed $\approx 14$ cm/s. (b) Velocity fluctuations are large only at the moments the interfaces of density discontinuity pass the observation boxes. As is visualized in Fig. 3(a), the abrupt change of longitudinal velocities leads to an ill-defined mean value for calculating $\delta V_x$ in each finite-sized observation box, which is $(9d \times 6d)$ in this case; therefore, the rms transverse fluctuation $\langle \delta V_y \rangle_{rms}$ may better represent the ''granular temperature.''

can be a significant fraction of the channel length. In this UDF, the upward propagation of the oscillation of local mean velocity can be estimated as faster than 100 cm/s.

The density for the UDF [shown in Fig. 7(b)] is always near the close-packing density. At this high density, a considerable fraction of beads can form temporarily rigid clusters, which lead to the long-range correlation and the fast propagation of local mean velocity mentioned above. More details about the microscopic structure of these dense regions are included in Sec. III D.

### C. Transverse profiles

To understand the response of the flow to shear forces imposed at the boundary, we study the transverse profiles. However, in either the UDF or the 2PF regime, the typical temporal oscillation of the mean velocity is comparable to or even larger than the velocity difference across the channel. For this reason, the usefulness of a simple long-time averaged profile may be questionable. Instead, we investigate the velocity profiles conditional on the local mean velocity.

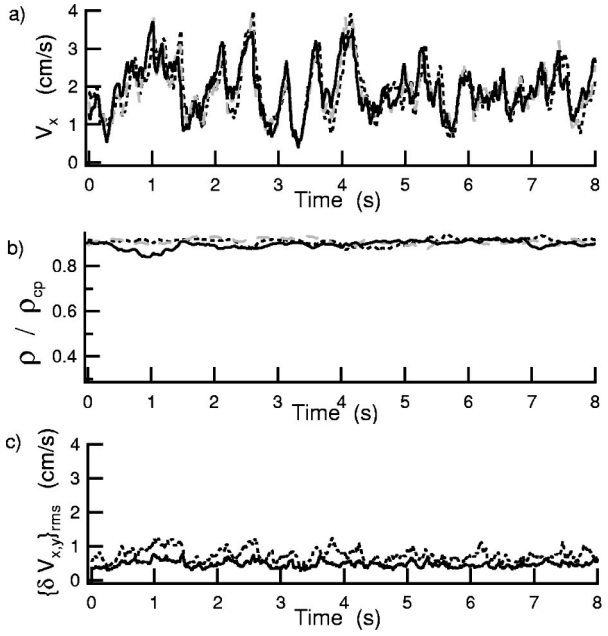


a,b) Mean velocity ($V_x$) and density (ρ) in three boxes along the channel:
------upstream, – – middle, ——downstream
c) RMS velocity fluctuations (the downstream box only) :
------longitudinal ( $\{\delta V_x\}_{rms}$ ) , ——transverse ( $\{\delta V_y\}_{rms}$ )

FIG. 7. Time dependence of a UDF with $W=12d$ and $D=3d$. The density is always near the 2D close-packing density $\rho_{cp}$. The local mean velocities in all observation boxes along the stream exhibit large irregular oscillations, which are almost simultaneous. The typical magnitude of rms velocity fluctuations is smaller than that of the mean velocity variations.

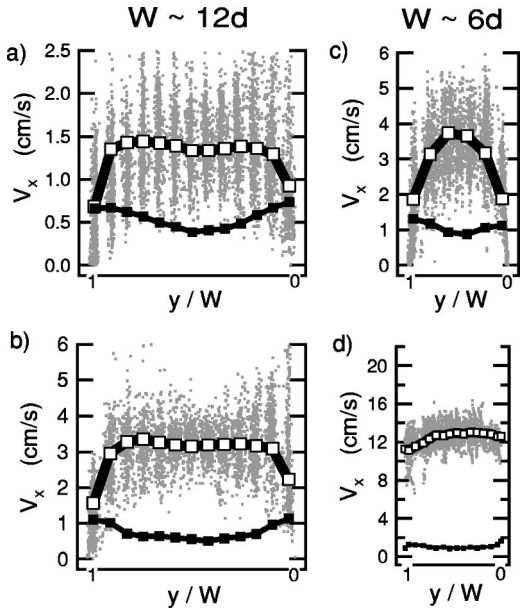


FIG. 8. Velocity profiles conditional on the local mean velocity, with $y/W$ being the normalized transverse position. The limits set on the local mean velocity are $\langle V_x\rangle_{snapshot}=(1.4\pm0.2)$ cm/s for (a), $(3.2\pm0.2)$ cm/s for (b), $(3.1\pm0.6)$ cm/s for (c), and $(12.5\pm0.6)$ cm/s for (d). Open symbols denote the conditionally averaged longitudinal velocity at each position, and filled symbols the corresponding statistical standard deviation. The background dots represent the velocities and positions of individual particles. (a,b) Wide-channel UDF with $W=12d$, $D=3d$: The same velocity plateau appears at different stages of oscillation. The transverse positions show strong layering preferences. (c,d) Narrow-channel 2PF with $W=6d$, $D=5d$: at a dense stage shown in (c), the velocity gradient penetrates the flow; at a free-fall stage shown in (d), large slips occur at the boundary and the velocity profile is relatively flat.

That is, we first consider all snapshots that have a mean velocity falling into a certain range, and we then obtain the conditional velocity profile by averaging over these snapshots only. The choices of observation boxes are similar to those used for studying oscillations (see Sec. III B).

In a wide channel with a UDF, the conditional average profiles [Figs. 8(a,b)] consist of a plug flow in the center plus shear bands at the edges. This is true at any stage of the oscillation, in spite of the considerable differences in mean velocity. This pattern matches the time-averaged velocity profiles established in previous investigations of wide-channel flows [1,3,4,6]. Our analysis shows that the time-averaged profile is the result of averaging similar conditional profiles. The occurrence of the velocity plateau at all mean velocities implies that in the plug region, starting at a distance $\approx 3d$ away from the side walls, beads acclerate/decelerate cooperatively. Further detail on this point will be presented in Sec. III D 4.

The velocity scatter plots in Figs. 8(a,b) show strong layering of individual transverse positions, which is a clear sign of crystallization due to the monodispersity. Nevertheless, the solidlike behavior is not unique to the monodisperse case. Our tests with binary mixtures of steel beads have shown qualitatively the same plug-flow profiles and cooperative velocity oscillations; however, other complications such as particles lifting off the plate due to the collisions of two differently sized rolling spheres also occur, raising a challenge for more detailed studies of binary mixtures.

The 2PF in a narrow channel exhibit distinct behaviors [Figs. 8(c,d)] at different stages of the oscillation. Figure 8(c) shows the ''dense stage'' of the 2PF and corresponds to the right hand side of the sample image Fig. 3(a). The velocity gradient caused by the boundary shearing penetrates the flow. On the other hand, Fig. 8(d) shows the ''free fall stage'' of the 2PF and corresponds to the left hand side of the sample image Fig. 3(a). The velocity profile is virtually flat due to the lack of contacts between the particles and the boundary; the measured velocity difference across the channel is mostly the ''memory'' of the initial time at which the beads were released from the dense region.

### D. Microscopic views of dense regions

Finer details concerning interactions between individual particles can be obtained by studying snapshots of bead motions and data on interparticle distances. We find that the dense regions can exhibit temporary arches, long-range correlated velocities, inhomogenuous propagation of disturbances, and local hexagonal structure. The explanation of these features may require advanced models that go beyond the conventional binary collision theory.

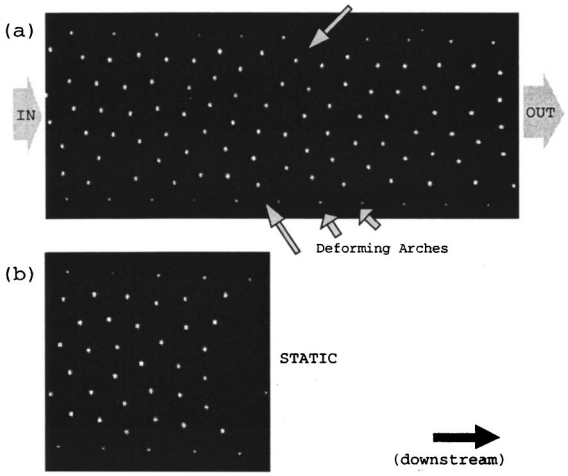


FIG. 9. (a) Temporary arching: the arch lines deform as particles rub against each other. (b) Permanent arching: when $W<6d$, enduring arches can occur and stop the flow. (The size of bright spots in the images does not represent the actual diameter of the steel beads.)

#### *1. Formation of temporary arches*

The formation of temporary arches, Fig. 9(a), becomes important when the width of the channel is smaller than about $9d$. A visual examination of the sequential images reveals that particles form temporary arches that are supported by the bumpy sidewalls and are continuously deforming as beads rub against their neighbors; beads along the arches are presumably contacting more than one neighbor and the main dynamics in the relaxation of these arches may be due to friction rather than collisions. In addition, as we decrease the channel width with the mean velocity fixed, both the likelihood of arch formation and its typical duration increase. This favors the creation of large-amplitude density waves. When the channel is narrower than $6d$, the occasional occurrence of permanent arching may stop the flow, as shown in Fig. 9(b). The flow consistently stops when the channel is narrower than $5d$. In a recent study, To *et al.* [28] conducted experiments on uniformly sized round disks flowing through the exit of a vertical 2D funnel, and found that the probability of permanent arching increases from zero to one as the exit width changes from $5d$ to $3d$.

#### *2. Correlated bead velocities*

The time dependence of velocity and its local fluctuation in a UDF [Fig. 7(a)] suggests that beads motions are correlated with a length scale at least several tens of bead diameters. With the aid of snapshots on grain positions and velocities, we further demonstrate that large parts of the flow exhibit hexagonal local lattices with defects. Figure 10 is a typical example with a dislocation line: across the line of dislocation, the beads appear to have a discontinuity in the preferred direction of velocity. Figure 11 reveals that the regional predominant velocity relative to the mean value over the field of view is preferentially aligned with the local lattice orientation.

To illustrate the effect of the long-range velocity correlation, we show the snapshot of a dense flow around an obstacle in Fig. 12. The typical size of the temporary pattern showing regional preferences in velocity is larger than the size of the obstacle. The apparent asymmetry of the pattern is not due to asymmetry of the geometry; it changes stochastically with time. In addition, the large slip around the obstacle and the void region behind it contrast with conventional fluid flows.

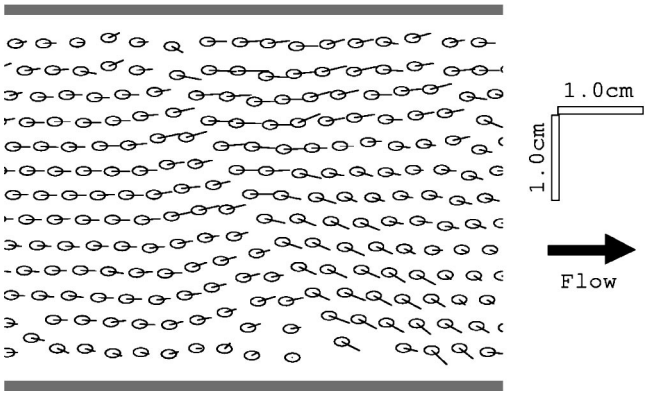


FIG. 10. Snapshot of a UDF with flags showing the individual velocities. $W=12d$, $D=5d$. Each flag points from the center of a bead along the direction of its velocity, with length proportional to the magnitude. Across the dislocation line, the velocity field exhibits a substantial change of preferred direction.

#### *3. Inhomogeneous propagation of velocity perturbations*

As shown in Fig. 13, we find that velocity perturbations in the dense regions can propagate in a very inhomogeneous way. The sequential development (continuously recorded for about 12 video frames in this case) shows that the disturbance, initiated at the lower middle of the field of view, develops a cracklike pattern across the channel. It is probable that the primary momentum transfer in these dense regions mimics the inhomogeneous stress chains observed in experiments using photoelastic disks [29–31] , rather than the dif-

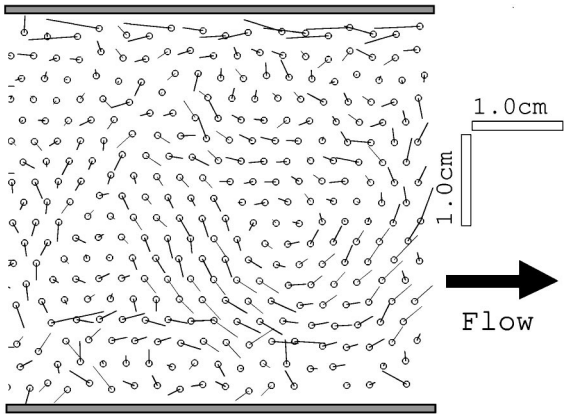


FIG. 11. Snapshot of a UDF with flags showing the deviation velocities, i.e., the velocities with the mean velocity of all particles in the field of view subtracted. $W=16d$, $D=4d$. The directions of individual deviation velocities are strongly correlated with the local lattice orientation. The pattern shown in the figure persists for about 0.04 s.

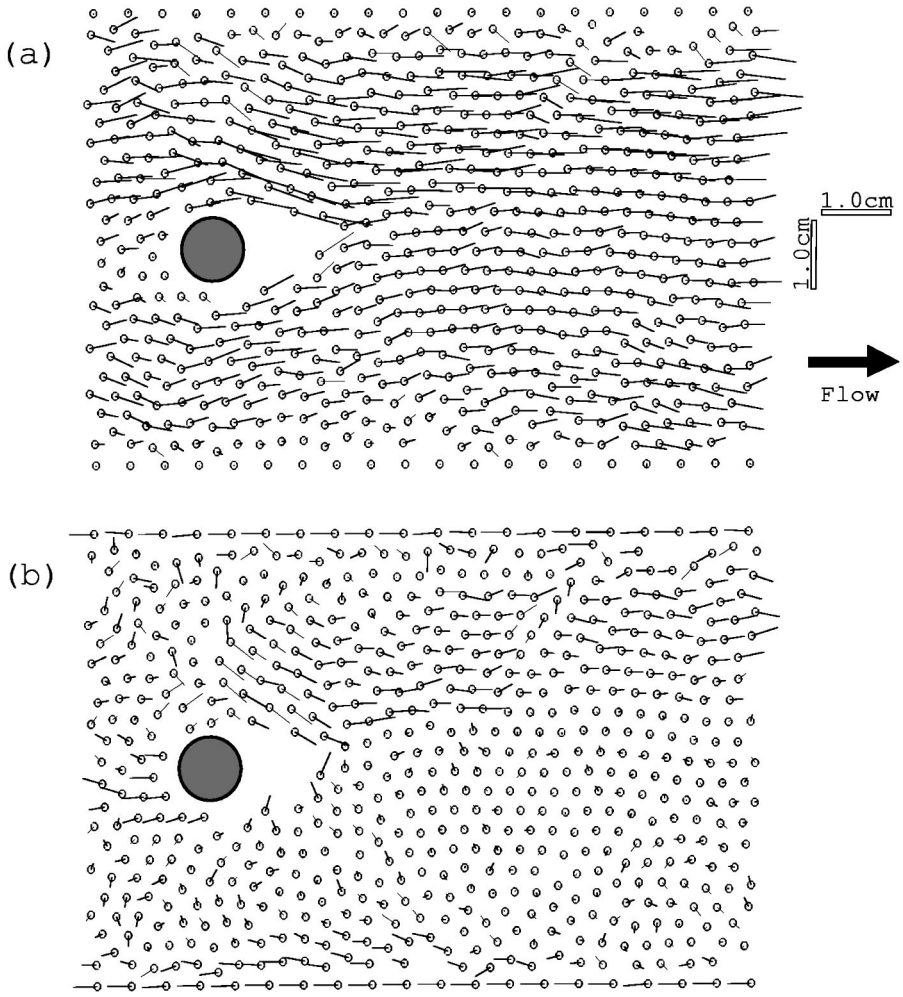


FIG. 12. Snapshots of a dense flow around an obstacle. The flow is bounded in a wide channel: (a) True velocities; (b) deviation velocities, i.e., the velocities with the mean velocity of all particles in the field of view subtracted. The pattern of the velocity field changes stochastically with time and is larger than the obstacle size.

fusive momentum transfer in situations similar to molecular gases. However, the finite instrumental resolution limits our ability to determine whether the sequential development is indeed produced by extremely small-amplitude binary collisions, or not.

#### *4. Nonballistic motion and the cage effect*

In order to understand the way beads approach and contact each other, we follow certain typical beads and investigate the time evolution of distances from their neighbors. In Fig. 14(a), we choose a reference bead in the plug-flow region of an UDF and plot the distances from its nearest neighbors as functions of time. Once their separations approach $1d$, they do not seem to oscillate much, presumably because the contacts are highly dissipative. Multiple curves corresponding to different neighbors coincide at around $1d$; this is consistent with a scenario where multiple neighbors make long-duration contacts. If there is any residual chattering, it is smaller than our image resolution $\approx 0.012d$ or $\approx 38\ \mu$m.

The cage effect, i.e., the long duration over which particles stay as nearest neighbors, explains the existence of the plug-flow profiles in a typical UDF. Figure 14(a) shows that the replacement of nearest neighbors in the center region is slow compared to the oscillation of the mean velocity [see Fig. 7(a)]. Since particles caged in these local lattices accelerate or decelerate collectively, this effect explains why the same shape of velocity plateau consistently appears throughout all stages of the large-amplitude velocity oscillations [Figs. 8(a,b)]. In contrast, the replacement of nearest neighbors occurs more frequently in the shear bands, as shown in Fig. 14(b). Figure 14(b) also illustrates the fact that all neighbors lose contact with the reference particle at certain moments; however, the curves still do not exhibit prominent ballistic reflections.

#### *5. Statistics of particle separations*

To understand the separation between particles and their nearest neighbors, we calculate the probabilities of finding at least two beads or at least three beads within distance $r$ from any chosen reference bead and present them in Fig. 15. The curves are obtained by integrating the histograms of the measured second or third nearest neighbor distances. In spite of the restriction of a finite image resolution, it can be inferred from Fig. 15(a) that, in the plug-flow region, over 80% of the beads have at least three neighbors that are either in contact or closer than the current image resolution ($\approx 0.012d$). In the shear band, on the other hand, only about 60% of the beads have more than three neighbors found within distance $(1+0.01)d$, as shown in Fig. 15(b).

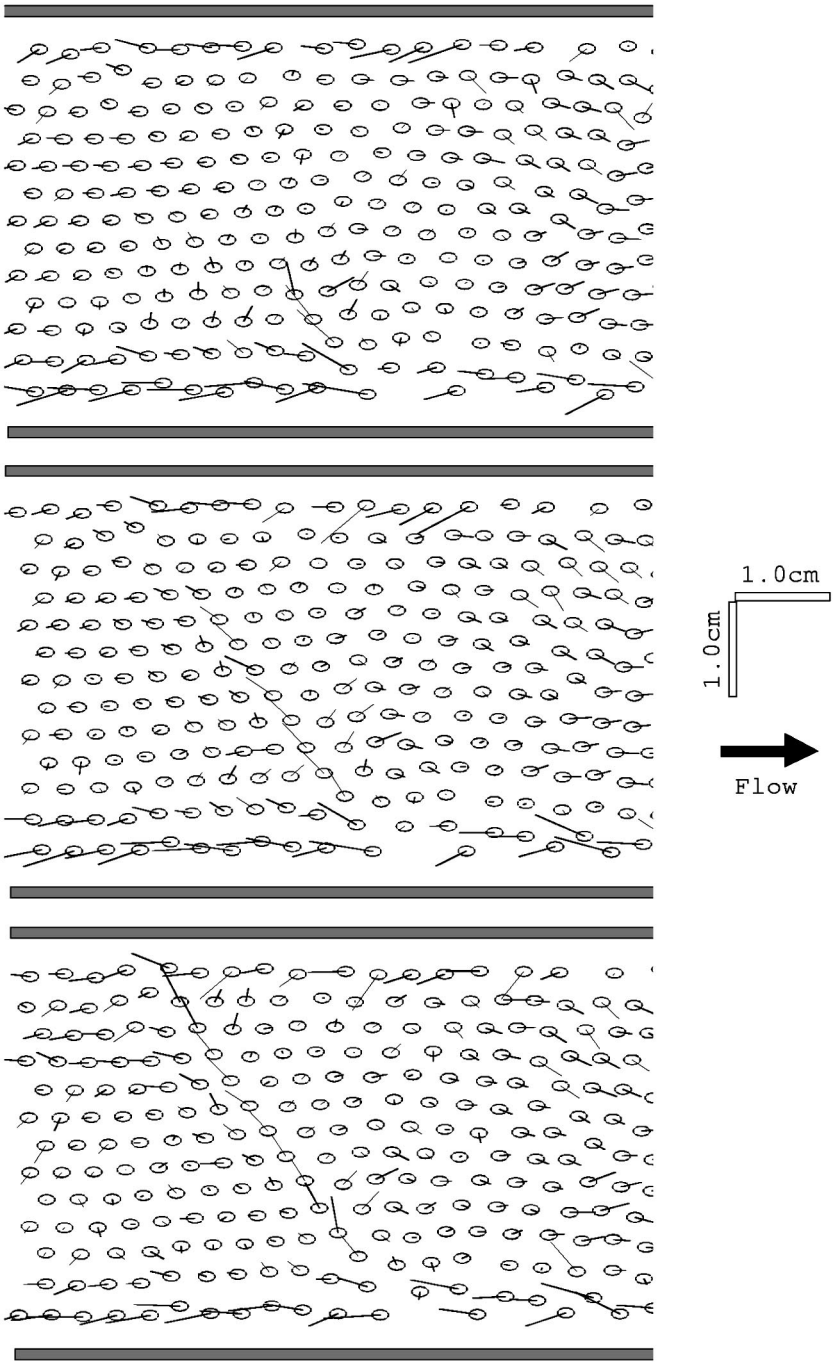


FIG. 13. Time series of snapshots, demonstrating the spatiotemporal evolution of a velocity perturbation. $W=12d$, $D=5d$. Individual flags show the deviation velocities, i.e., the velocities with the mean velocity of all particles in the field of view subtracted. Initiated at the lower middle of the field of view, a cracklike pattern develops across the channel, with deviation velocities pointing approximately in the same direction. The development of the cracklike pattern spans about 12 frames at a time interval of 0.008 s; three representative snapshots, which are 0.024 s apart, are displayed from top to bottom. The sequential development of the pattern suggests that momentum can be transferred in a highly inhomogeneous way.

At a larger scale, we calculate the histogram of center-to-center distances of all beads in a plug-flow region of a UDF and present it in Fig. 16. The peaks at $1d$, $\sqrt{3}d$, $2d$, . . . correspond to those expected in a hexagonal lattice, which results from the monodispersity. The peaks are broadened because the hexagonal lattice structures experience stochastic deformation. Interestingly, the noninteger peaks are wider than the integer peaks. This fact can be consistently explained if we assume a scenario in which sliding contacts prevail: as neighbors rub against each other, a considerable fraction of interparticle contacts are preserved during a small deformation of the lattice. For an infinitesimal sliding deformation of a perfect hexagonal lattice, this would presumably cause a second-order perturbation to the width of integer peaks of the pair-distance distribution function, whereas the effect on the noninteger peaks would be first order. We speculate that detailed analysis of the shape of the pair-distance distribution function could lead to some insight into the collective motion in the dense regions. Extensive discussions by previous researchers on the dynamics of spheres with prevalent crystalline ordering can be found in Ref. [14] and the references therein.

## IV. SUMMARY AND DISCUSSION

Here we summarize our findings concerning the dynamics of 2D monolayer granular flows on an incline. We find that

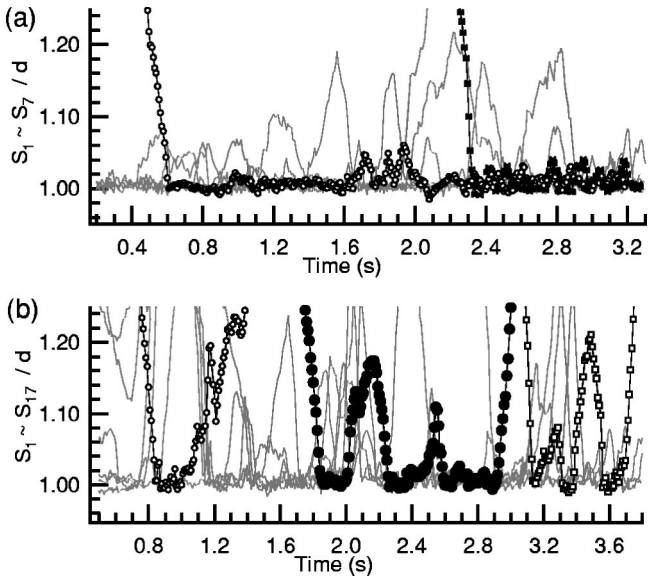


FIG. 14. Separations of neighbors as functions of time. $W=12d$, $D=3d$. The distance $S_i$ is measured from the center of the $i$th neighbor to the center of the selected reference bead, and is normalized by the bead diameter $d$. Separations of some typical neighbors are labeled with different symbols to guide the eye, and the unlabeled curves represent all the other neighbors. (a) The reference bead is in the plug-flow region: the replacement of the six nearest neighbors is rare—only once in this 3.1 s interval, which is sufficient for several oscillations of the local mean velocity [shown in Fig. 7(a)]. (b) The reference bead is in the shear band: nearest neighbors are replaced more frequently—17 different beads alternatively appear during the same amount of time. Note that at $t \approx 2.07$ s, all neighbors are at least $0.02d$ away from this reference bead. None of the curves in (a) or (b) exhibit prominent ballistic reflections.

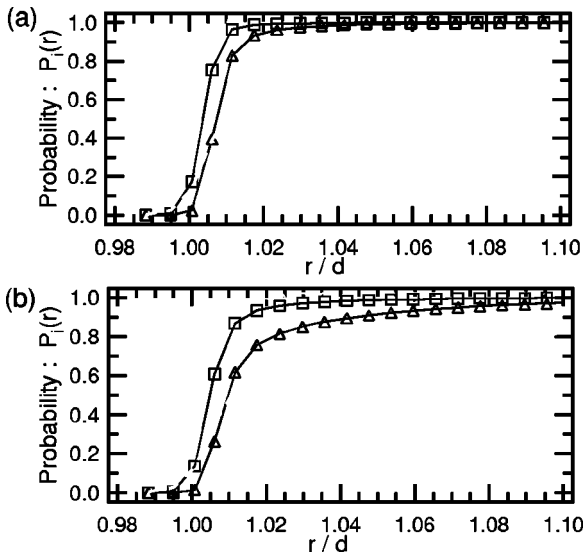


FIG. 15. $P_i(r) \equiv$ Probability of finding at least $i$ beads within the distance $r$ from the center of any reference bead. $P_2(r)$ is denoted by squares and $P_3(r)$ is denoted by triangles. $W=12d$, $D=3d$. (a) Plug-flow region; (b) shear band, where the curves rise somewhat more slowly.

an open channel results either in a dilute accelerating flow with a mean flow rate determined by inlet conditions, or causes a static jammed solid supported by the sidewalls when the channel is narrower than about five bead diameters. In an exit-constricted channel with a certain range of exit widths, flows that do not accelerate (in a time-averaged sense) down the channel can be obtained; we call these fully developed flows. We have established that there is a continuous transition between two distinct regimes—UDF and oscillatory 2PF—depending on the channel width $W$ and the mean flow velocity (Figs. 2 and 5). The rough boundary is identified as a necessary condition to cause the transition. The two regimes have quite different patterns of density and velocity oscillations (Figs. 6 and 7), and flow profiles (Fig. 8). Both regimes exhibit large-amplitude oscillations of coarse-grained velocity, which propagate upstream with considerably different speeds depending on the flow regime.

In the dense regions of both regimes, the observations may require models that go beyond the standard binary collision approaches. Specifically, the dense regions are cold in the sense that velocity fluctuations are smaller than the typical time variation of local mean velocity. Temporary arches occur in the 2PF through narrow channels (Fig. 9). Correlated grain motions with length scale comparable to the system size are observed in wide-channel UDFs (Figs. 10, 11, and 12). Disturbances of the velocity field can propagate in a very inhomogenous way (Fig. 13). The time evolution (Fig. 14) of particle separations reveals that, in dense flows, particle motions are nonballistic and the replacement of nearest neighbors is slow compared to the oscillation of the mean velocity. Statistics of interparticle distances (Figs. 15 and 16) show that multiple close neighbors are prevalent and that the dense regions are largely crystallized.

We consider certain important features of our flows and compare our results with previous investigations of 2D granular Poiseuille flow before concluding the discussion.

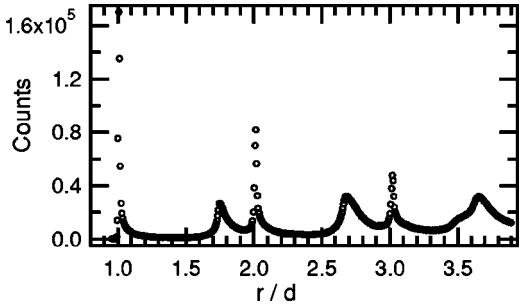


FIG. 16. Histogram of center-to-center distances in the plug-flow regions of UDF with $W=12d$ and $D=3d$. Reference beads are collected from a $(4d \times 27d)$ rectangular region defined symmetrically along the center line of the flow. The statistics include 1000 snapshots spanning 8 s, which is much longer than the time scale corresponding to the oscillation of the coarse-grained mean velocity [shown in Fig. 7(a)]. The peaks at $1d$, $\sqrt{3}d$, $2d$, ... correspond to those of a hexagonal lattice. The noninteger peaks are much broader than the integer peaks.

### A. Density waves in narrow channels

In high-speed flows developed in a narrow channel that is constricted at the exit, we consistently find two-phase flows (Fig. 3) characterized by strong density waves propagating backwards. Here we provide a phenomenological explanation of why a homogeneous high-density flow cannot exist at a higher mean flow velocity. Consider a uniform, nearly close-packing base state with a constant mean velocity and a finite velocity fluctuation. Suppose the density field is perturbed by a small modulation along the stream. The denser regions have a dramatic increase in collision rate since it is inversely proportional to the average gaps left between spheres. Therefore, the collisional resistance at the boundary causes the dense region to decelerate. Also the high collisional dissipation may bring a fraction of beads into long-duration contacts, which can have several effects including temporary arching or turning closely rolling beads into a rigid cluster sliding against the bottom plate. All of these effects tend to enhance the deceleration and cause local congestion. The congestion then gradually relaxes from the downstream side and beads accelerate until reaching the next point of local congestion.

The monotonic relation between the density wave amplitude $\delta\rho_{rms}$ and the time-averaged velocity $\langle V_x\rangle$ (see Fig. 5) can be understood as follows. First, Fig. 6(a) indicates that the congested regions contribute to a small fraction of each typical oscillation cycle and have a much smaller mean velocity compared to other regions, where beads almost freely accelerate. Therefore, the time average $\langle V_x\rangle$ should predominately scale with the characteristic time of these congestion-relaxation cycles. Second, $\delta\rho_{rms}$ should scale with the typical difference between the maximum and minimum density, where the maximum is approximately the close-packing density $\rho_{cp}$ and the minimum is primarily determined by the volume expansion during the relaxation acceleration. Thus, it is expected that $\delta\rho_{rms}$ scales with the same characteristic time mentioned above and consequently has a monotonic dependence on $\langle V_x\rangle$.

The traditional binary-collision theories described in Sec. I B may have limited applicability to the strong density waves we observe. In the dilute regions, particles may experience less than one collision before reaching the next congested region, as a combined effect of small velocity differences between neighbors and long mean free path (Sec. III B). In the dense regions, the presence of temporary arches suggests frictional dynamics where contacts involving more than two particles should be an important factor. Significant velocity fluctuations only exist at the interfacial region of density discontinuity and dissipate quickly. As a result, calculations assuming a ''local equilibrium'' required by these theories resembling molecular gases may not approximate the situation well.

### B. Consideration of finite-length effects

The channel has an inlet and an exit, and thus differs from an idealized infinitely long channel. Over the entire range of those statistically steady flows, we have found that the jamming extends all the way back into the hopper, and that the wave propagation is always backwards. Therefore, the inlet condition does not seem to influence the flow, unless the feeding rate is so low that the flow transforms into accelerating gas. However, one may speculate that the exit could possibly influence the density oscillation.

In the oscillatory 2PF limit, the constriction at the exit plays the role of maintaining the time-averaged density so as to prevent AGF. However, the exit's effect on the *oscillation* of density and velocity, if any, should be insignificant compared to the effect of the rough boundaries for the following reasons.

(1) Tests using flat boundaries (Sec. III A) show that the occurrence of density waves is much more sensitive to the roughness of the wall than it is to the geometrical factors $W$ and $D$.

(2) Additional observations show that significant amplitude of the upward-traveling waves develops typically at least 20 cm away from the exit, and that the characteristic time scale for the traveling waves is much longer than that of the seemingly irregular perturbations at the exit. The disturbances at the exit do not seem to propagate beyond the ''exit zone.''

(3) Interestingly, our observations are qualitatively similar to Sanders and Ackermann's molecular dynamics (MD) simulations [20] of flows in a periodic narrow channel ($W=3d$), which is meant to resemble an idealized infinite channel. Their simulation shows density waves similar to those in our 2PFs; they have found that the typical length of the densely packed regions depends on the inelasticity of the colliding grains and the bumpy boundary.

On the other hand, in the UDF regime where the oscillation of density is minor, the exit condition may have substantial effects on the oscillation of the velocity. In this dense regime, particles can have long chains of contacts, and the range of correlated motion can be comparable to the length of the channel. It is reasonable to believe that normal stresses and their fluctuations can be transmitted from the exit up the entire channel.

### C. Comparison to other experiments

Veje, Hørlück, and Dimon [7–9] have extensively studied the flows of monolayer brass beads ($d=0.3175$ cm) rolling through a long small-angle 2D funnel built on a flat incline. Unlike our rough boundaries, their funnel walls are smooth. They established [7] that, using an inclination $\theta=4.1°$ and keeping the funnel exit fixed as 1 cm, the general behavior can be divided into three regimes characterized by the funnel half-angle $\beta$: ''(i) pipe flow'' (at $\beta<0.1°$) where the flow is relatively dilute and density waves tend to stay stationary or vanish before reaching the inlet; (ii) ''intermittent flow'' ($0.1°<\beta<\sim 1°$) where density discontinuities propagate upwards through the entire channel; and (iii) ''dense flow'' [32] (at larger $\beta$, typically up to 2° or 3°) where the density is close to $\rho_{cp}$ with a rather weak variation, and fast propagation of velocity disturbances are observed.

Similarities can be found in comparing their ''intermittent flow'' to our 2PF regime, and in comparing their ''dense flow'' to our UDF regime [33]. However, the rough bound-

aries in our experiment create most of the differences.

(1) In our 2PFs, the strong density waves are predominantly triggered by the sidewalls (discussed in Sec. IV B); while in their intermittent funnel flows with funnel angle $\beta \geqslant 0.2°$, the ''dilatant fluctuations at the exit'' contribute to generation of density waves [7].

(2) Our rough walls trigger disturbances to the flow with an equal likelihood everywhere along the entire channel, whereas their investigation on the behavior of velocity shock fronts [8] shows that their density waves are preferentially initiated at ''packing sites,'' i.e., the locations with a local funnel width equal to multiples of the bead diameter.

(3) Our transverse profiles (Fig. 8) reveal the interaction with the boundary in contrast to their experiment where the shear interaction is negligible.

Experimental studies of thin or monolayer granular flows in vertical chutes provide another category for comparison. Strong density waves similar to that of our 2PFs are also reported in the work of Clement *et al.* [11] on monolayer flows through a vertical 2D channel with rough sidewalls. This assures us that density waves are not unique to rolling bead flows and that the rough boundary is the key factor triggering the density waves. On the other hand, in our UDFs, where strong density waves are absent, the mechanism that causes the large-amplitude oscillations of instantaneous mean velocity still calls for further understanding. Many of the previous investigations of granular flows in wide vertical chutes [1,3,6,4] report nearly steady flow profiles with channel widths and sidewall roughness comparable to ours (in units of particle diameter); most of them [1,3,6] have a narrow exit serving as a flow control valve as in our setup. The investigated range of particle size and velocity in these previous experiments overlaps with our investigation. Whether the large oscillation of the mean velocity in our UDFs is generic to gravity-driven Poiseuille flows with a reduced value of $g$ or results from the rolling dynamics is not obvious.

## V. CONCLUDING REMARKS

The primary factors controlling the general behavior of the inclined 2D Poiseuille flows include the exit width, the channel width, and the roughness of the sidewalls. Collisions with the bumpy sidewalls are essential for triggering strong density waves in the flows developed in constricted channels. However, the passive collisions at the sidewall do not provide sufficient drag to eliminate acceleration in the dilute (gaseous) regions.

In all cases where dense regions emerge, the particle motion shows long-range correlations and local ordering; a complete model would need to go beyond conventional kinetic methods for granular systems of moderate density. In the dilute regions of our flow, conventional kinetic theories are inappropriate—the mean free path exceeds the channel width and the mean collision interval is comparable to the typical travel time between dense regions. Moreover, the presence of strong density waves means that the local dynamics constantly switch back and forth between a dense creeping state and a nearly-collision-free accelerating state. Existing paradigms can successfully describe a number of granular systems having relatively less spatial and temporal density variations than found here. However, a significant extension of current theories, or a different approach, will be needed to understand granular flows that spontaneously develop inhomogeneity so strong as to show contrasting dynamical features at different locations or at different times.

## ACKNOWLEDGMENTS

This work was supported by the National Science Foundation under Grant No. DMR-00-79909 to the University of Pennsylvania and Contract No. DMR-0072203 to Haverford College. We appreciate helpful conversations with J. Jenkins and T. Lubensky. R. Amit contributed to the early stages of this investigation. We are grateful to B. Boyes for his continual technical assistance.

[1] R. Nedderman and C. Loahakul, Powder Technol. **25**, 91 (1980).
[2] S. B. Savage, J. Fluid Mech. **92**, 53 (1979).
[3] S. B. Savage, Adv. Appl. Mech. **24**, 289 (1984).
[4] O. Pouliquen and R. Gutfraind, Phys. Rev. E **53**, 552 (1996).
[5] M. Hunt and S. Hsiau, in *Advances in Micromechanics of Granular Materials*, edited by H. H. Shen *et al.* (Elsevier Science, Amsterdam, 1992), pp. 141–150.
[6] V. Natarajan, M. Hunt, and E. Taylor, J. Fluid Mech. **34**, 1 (1995).
[7] C. T. Veje and P. Dimon, Phys. Rev. E **54**, 4329 (1996).
[8] S. Hørlück and P. Dimon, Phys. Rev. E **60**, 671 (1999).
[9] S. Hørlück and P. Dimon, Phys. Rev. E **63**, 031 301 (2001).
[10] T. Raafat, J. P. Hulin, and H. J. Herrmann, Phys. Rev. E **53**, 4345 (1996).
[11] G. Reydellet, F. Rioual, and E. Clement, Europhys. Lett. **51**, 27 (2000).
[12] R. Bagnold, Proc. R. Soc. London, Ser. A **225**, 49 (1954).
[13] C. S. Campbell, Annu. Rev. Fluid Mech. **22**, 57 (1990).
[14] S. Luding, Phys. Rev. E **63**, 042 201 (2001).
[15] K. Hui and P. Haff, Int. J. Multiphase Flow **12**, 289 (1986).
[16] S. B. Savage, J. Fluid Mech. **377**, 1 (1998).
[17] A. Valance and T. LePennec, Eur. Phys. J. B **5**, 223 (1998).
[18] J. Jenkins, Appl. Mech. Rev. **47**, S240 (1994).
[19] C.-H. Wang, R. Jackson, and S. Sundaresan, J. Fluid Mech. **342**, 179 (1997).
[20] B. E. Sanders and N. L. Ackermann, in *Advances in Micromechanics of Granular Materials* (Ref. [5]).
[21] S. Luding, J. Duran, E. Clement, and J. Rajchenbach, J. Phys. I **6**, 823 (1996).
[22] J. Duran, T. Mazozi, S. Luding, E. Clement, and J. Rajchenbach, Phys. Rev. E **53**, 1923 (1996).
[23] B. Painter and R. P. Behringer, Phys. Rev. E **62**, 2380 (2000).
[24] D. L. Blair and A. Kudrolli, e-print cond-mat/0101015.
[25] The computing routines were previously developed by J. Crocker, E. Week, and W. Losert.

[26] J. Crocker and D. Grier, J. Colloid Interface Sci. **179**, 298 (1996).
[27] http://www.haverford.edu/physics-astro/Gollub/2D_granular.html
[28] K. To, P.-Y. Lai, and H. K. Pak, Phys. Rev. Lett. **86**, 71 (2001).
[29] A. Drescher and G. De Josselin De Jong, J. Mech. Phys. Solids **20**, 337 (1972).
[30] R. Behringer and G. Baxter, in *Granular Matter*, edited by A. Mehta (Springer-Verlag, New York, 1994), pp. 85–119.
[31] D. Howell, R. P. Behringer, and C. Veje, Phys. Rev. Lett. **82**, 5241 (1999).
[32] Here we adopt the term ''dense flow'' in accordance with the usage in the authors' later publications that refer to this experiment.
[33] In these experiments, the exit width is fixed as $\approx 3.1d$; at a typical funnel angle $\beta = 2°$ the funnel width in the middle of their 2-m-long channel is about $20d$. Thus, the conditions are comparible to the small exit width and wide channel for our UDFs.